Article

To Be or Not to Be a (4,4) Net: Reactions of 4'-{4-(*N,N*-Diethylaminophenyl)}- and 4'-{4-(*N,N*-Diphenylaminophenyl)}-3,2':6',3''- and 4,2':6',4''-Terpyridines with Cobalt(II) Thiocyanate

Dalila Rocco [†] [ID], **Anamarija Nikoletić** [†] [ID], **Alessandro Prescimone** [ID], **Edwin C. Constable** [ID] **and Catherine E. Housecroft** *[ID]

Department of Chemistry, University of Basel, Mattenstrasse 24a, BPR 1096, 4058 Basel, Switzerland
* Correspondence: catherine.housecroft@unibas.ch
† These authors contributed equally to this work.

Abstract: The ligands 4'-{4-(*N,N*-diethylaminophenyl)}-3,2':6',3''-terpyridine (**1**) and 4'{4-(*N,N*-diphenylaminophenyl)}-3,2':6',3''-terpyridine (**2**) were prepared and characterized, including the single crystal structure of **2**. Along with their 4,2':6',4''-terpyridine isomers, **3** and **4**, ligands **1** and **2** were reacted with Co(NCS)$_2$ under conditions of crystal growth by layering, using solvent mixtures of MeOH and CHCl$_3$. The single crystal structures of [Co(NCS)$_2$(**1**)]$_n$·0.8nCHCl$_3$, [Co(NCS)$_2$(**2**)$_2$(MeOH)$_2$]·3CHCl$_3$, [Co(NCS)$_2$(**3**)]$_n$·2nCHCl$_3$, and [Co(NCS)$_2$(**4**)]$_n$ were determined. The complexes with **1**, **3**, and **4** assemble into 2D (4,4) nets with the Co(II) centres as 4-connecting nodes, whereas [Co(NCS)$_2$(**2**)$_2$(MeOH)$_2$] is a discrete molecular species, illustrating that MeOH can act as a non-innocent solvent. The effects on the structure of changing from the 3,2':6',3''-terpyridine (3,2':6',3''-tpy) to a 4,2':6',4''-tpy metal-binding unit, and of introducing R$_2$N functionalities with different steric demands, are discussed. PXRD of bulk samples of all four products confirmed the single-crystal structures as representative of the bulk materials.

Keywords: 3,2':6',3''-Terpyridine; cobalt(II) thiocyanate; (4,4) net; R$_2$N functionalities

1. Introduction

The 4,2':6',4''-terpyridine (4,2':6',4''-tpy) metal-binding domain has increased in popularity as a building block in coordination polymers and networks, while 3,2':6',3''-terpyridines (3,2':6',3''-tpy) are less well examined [1–4]. The introduction of functional groups in the 4'-position of the tpy unit is synthetically straightforward, and provides a means of tuning the properties of the ligands and their coordination complexes. Among the coordinatively innocent functionalities introduced into 4,2':6',4''- and 3,2':6',3''-tpy ligands, *N,N*-diarylamino and *N,N*-dialkylamino substituents have received attention because of the donor–acceptor (D–A) nature of 4'-{4-(*N,N*-diarylaminophenyl)}terpyridines and their photophysical properties [5,6]. Similar D–A behaviour is observed for derivatives containing (EtO$_2$CCH$_2$)$_2$NC$_6$H$_4$ substituents [7]. Structural and catalytic properties have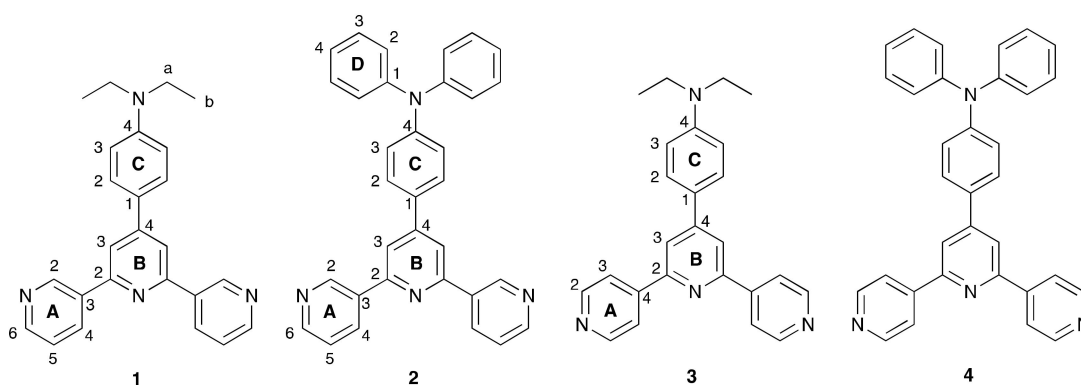 been the focus of a number of investigations of metal coordination compounds incorporating 4'-(4-R$_2$NC$_6$H$_4$)-4,2':6',4''-terpyridines [8–15]. Reports of structurally characterized coordination polymers incorporating 4'-(4-R$_2$NC$_6$H$_4$)-4,2':6',4''-tpy ligands are restricted to *N,N*-dimethylaminophenyl derivatives [13,16].

Our recent investigations into the formation of (4,4) nets assembled from 3,2':6',3''-tpy ligands and Co(NCS)$_2$ illustrated both the conformational flexibility of the 3,2':6',3''-tpy unit (Scheme 1) and the effects of introducing different alkyloxy substituents in the 4'-position of the 3,2':6',3''-tpy ligand [17–19]. We also noted the role that different lattice solvents play

in assemblies arising from a combination of $Co(NCS)_2$ and 4′-{4-(naphthalen-1-yl)phenyl}-3,2′:6′,3″-terpyridine [20]. Use of a coordinating solvent, such as MeOH, in crystallization experiments can lead to competition for cobalt(II) coordination sites, militating against the assembly of a 2D-network [21]. In the current work, we investigated how the introduction of 4′-(*N*,*N*-diethylaminophenyl) or 4′-(*N*,*N*-diphenylaminopheny)l groups into 3,2′:6′,3″-tpy (ligands **1** and **2**, Scheme 2) affects the outcome of reactions with $Co(NCS)_2$; these substituents have significantly different steric demands, and the Ph_2N group also offers the potential for π-stacking interactions in the solid state. Analogous reactions were carried out using ligands **3** and **4**, which contain 4,2′:6′,4″-tpy units (Scheme 2).

Scheme 1. Limiting planar conformations of 3,2′:6′,3″-tpy.

Scheme 2. Structures of ligands **1**–**4**, with atom labelling, used for NMR spectroscopic assignments of **1**, **2**, and **3**. The NMR spectroscopic data for **4** have previously been reported [8,15].

2. Materials and Methods

2.1. General

^{1}H and ^{13}C{^{1}H} NMR spectra were recorded at 298 K on a Bruker Avance III-500 NMR spectrometer. ^{1}H and ^{13}C chemical shifts were referenced to residual solvent peaks with respect to δ(TMS) = 0 ppm. Matrix-assisted laser desorption ionization (MALDI) mass spectra were recorded using a Shimadzu MALDI-8020 instrument, without a matrix added during sample preparation. Absorption and infrared (IR) spectra were recorded on a Shimadzu UV2600 spectrophotometer and PerkinElmer UATR Two instruments, respectively.

Compounds **3** and **4** have previously been reported [8,11,15].

2.2. Compound **1**

4-(*N*,*N*-Diethylamino)benzaldehyde (1.77 g, 10.0 mmol) was dissolved in EtOH (50 mL), after which 3-acetylpyridine (2.42 g, 2.2 mL, 20.0 mmol) and crushed KOH (1.13 g, 20.0 mmol) were added to the solution. Aqueous NH_3 (32%, 38.5 mL) was slowly added to the reaction mixture, and this was then stirred at room temperature overnight (ca. 15 h). The solid that formed was collected by filtration and washed with H_2O and EtOH. The yellow product was dissolved in EtOH and left in the refrigerator (ca. 5 °C) to crystallize. The solid was collected by filtration and dried under vacuum. Compound **1** was isolated as a yellow solid (1.15 g, 3.03 mmol, 30.3%). M.p. = 161 °C. ^{1}H NMR (500 MHz, CDCl$_3$): δ/ppm 9.35 (d, J = 2.4 Hz, 2H, H^{A2}), 8.66 (dd, J = 4.8, 1.7 Hz, 2H, H^{A6}), 8.46 (dt, J = 8.0, 2.0 Hz, 2H, H^{A4}), 7.87 (s, 2H, H^{B3}), 7.64 (m, 2H, H^{C2}), 7.41 (dd, J = 7.9, 4.7 Hz, 2H, H^{A5}), 6.77 (m, 2H, H^{C3}), 3.41 (q, J = 7.1 Hz, 4H, H^a), 1.20 (t, J = 7.1 Hz, 6H, H^b). ^{13}C{^{1}H} NMR (126 MHz, CDCl$_3$): δ/ppm 155.1 (C^{A3}), 150.5 (C^{B4}), 150.0 (C^{A6}), 148.8 (C^{C4}), 148.5 (C^{A2}), 135.1 (C^{B2}), 134.5 (C^{A4}),

128.1 (C^{C2}), 123.8 (C^{C1}), 123.6 (C^{A5}), 116.2 (C^{B3}), 111.8 (C^{C3}), 44.5 (C^{a}), 12.6 (C^{b}). UV-Vis (CH_2Cl_2, 2×10^{-5} mol dm^{-3}) λ/nm (ε/dm^3 mol^{-1} cm^{-1}): 273 (20,390), 293sh (16,600), 358 (23,000). MALDI-MS *m/z* 381.16 [M + H]$^+$ (calc. 381.21). Found C 78.32, H 6.32, N 14.62; required for $C_{25}H_{24}N_4$ C 78.92, H 6.36, N 14.73.

2.3. Compound **2**

4-(*N*,*N*-Diphenylamino)benzaldehyde (2.73 g, 10.0 mmol) was dissolved in EtOH (80 mL) and 3-acetylpyridine (2.42 g, 2.2 mL, 20.0 mmol) and crushed KOH (1.13 g, 20.0 mmol) were added to the solution. Aqueous NH_3 (32%, 38.5 mL) was slowly added to the reaction mixture, which was then stirred at room temperature overnight (ca. 15 h). The solid that formed was collected by filtration and washed with H_2O and EtOH. The yellow product was dissolved in EtOH/$CHCl_3$ and left to stand in a refrigerator (ca. 5 °C) to crystallize. The solid was collected by filtration and dried under vacuum. Compound **2** was isolated as a yellow crystalline solid (1.48 g, 3.11 mmol, 31.1%). M.p. = 227 °C. ^{1}H NMR (500 MHz, $CDCl_3$): δ/ppm 9.37 (d, *J* = 2.3 Hz, 2H, H^{A2}), 8.69 (dd, *J* = 4.8, 1.7 Hz, 2H, H^{A6}), 8.49 (dt, *J* = 8.0, 2.0 Hz, 2H, H^{A4}), 7.92 (s, 2H, H^{B3}), 7.62 (m, 2H, H^{C2}), 7.44 (dd, *J* = 8.0, 4.8 Hz, 2H, H^{A5}), 7.31 (dt, *J* = 7.4, 2.0 Hz, 4H, H^{D3}), 7.21–7.15 (overlapping m, 6H, H^{C3+D2}), 7.10 (m, 2H, H^{D4}). ^{13}C{^{1}H} NMR (126 MHz, $CDCl_3$): δ/ppm 155.4 (C^{A3}), 150.33 (C^{B4}), 150.26 (C^{A6}), 149.4 (C^{C4}), 148.5 (C^{A2}), 147.3 (C^{D1}), 134.9 (C^{B2}), 134.6 (C^{A4}), 131.0 (C^{C1}), 130.0 (C^{D3}), 128.0 (C^{C2}), 125.2 (C^{D2}), 123.9 (C^{D4}), 123.7 (C^{A5}), 122.9 (C^{C3}), 117.1 (C^{B3}). UV-Vis (CH_2Cl_2, 2×10^{-5} mol dm^{-3}) λ/nm (ε/dm^3 mol^{-1} cm^{-1}): 242 (28,020), 292 (18,780), 363 (17,850). MALDI-MS *m/z* 476.13 [M]$^+$ (calc. 476.20). Found C 81.62, H 4.98, N 11.41; required for $C_{33}H_{24}N_4$ C 83.17, H 5.08, N 11.76.

2.4. Crystallography

Single crystal data were collected on a STOE StadiVari Eulerian 4-circle diffractometer (CuKα radiation) equipped with a Dectris Eiger2 1M detector. Structures were solved using Superflip [22,23] and Olex2 [24]. The model was refined with ShelXL v. 2018/3 [25]. All H atoms were included at geometrically calculated positions and refined using a riding model with U_{iso} = 1.2 of the parent atom. Structure analysis and structural diagrams used CSD Mercury 2022.1.0 [26]. In [Co(NCS)$_2$(**1**)]$_n$·0.8*n*CHCl$_3$, the pyridine ring containing N1 is disordered, and was modelled over two sites of fractional occupancies, 0.45 and 0.55; the NEt$_2$ unit is also disordered, and was modelled over two equal occupancy sites. In [Co(NCS)$_2$(**2**)$_2$(MeOH)$_2$]·3CHCl$_3$, a solvent mask was used to treat part of the solvent region, and electrons removed corresponded to one CHCl$_3$ per formula unit. All the crystals of [Co(NCS)$_2$(**4**)]$_n$ were twinned, and the crystal selected for structure determination was indexed with two domains.

PXRD data were collected at 295 K in transmission mode using a Stoe Stadi P diffractometer equipped with a CuKα1 radiation (Ge(111) monochromator and a DECTRIS MYTHEN 1 K detector. Whole-pattern profile matching analysis [27–29] of the diffraction patterns was carried out using FULLPROF SUITE (v. January 2021) [29,30] and applying a previously determined instrument resolution function based on a NIST640d standard. The structural models were derived from the single crystal X-ray diffraction data. The refined parameters in the Rietveld analysis were scale factor, zero shift, lattice parameters, background points, and peak shapes as a Thompson-Cox-Hastings pseudo-Voigt function. Preferred orientations as a March–Dollase multi-axial model were used in the analysis.

2.5. Crystal Growth of the Coordination Complexes

A solution of Co(NCS)$_2$ (5.25 mg, 30 μmol) in MeOH (5 mL) was layered over a CHCl$_3$ solution (4 mL) of compound **1**, **2**, **3,** or **4** (11.4 mg of **1** or **3**, 30 μmol; or 14.3 mg of **2** or **4**, 30 μmol) in a sealed test-tube. X-ray quality crystals grew within 5 days. After selection of an X-ray quality crystal and structural determination, the remaining crystals were removed by fitration, and were washed with MeOH and CHCl$_3$, dried and analysed by PXRD and FT-IR spectroscopy.

2.6. Compound *2*

$C_{33}H_{24}N_4$, M_r = 476.56, colourless plate, monoclinic, space group C2/c, a = 34.855(5), b = 8.6116(8), c = 30.178(5) Å, β = 146.585(7)°, V = 4988.2(12) Å^3, D_c = 1.269 g cm^{-3}, T = 150 K, Z = 8, μ(CuK$_\alpha$) = 0.589 mm^{-1}. Total 36,601 reflections, 4524 unique (R_{int} = 0.0744). Refinement of 3249 reflections (335 parameters) with I > 2σ(I) converged at final R_1 = 0.0975 (R_1 all data = 0.1376), wR_2 = 0.2194 (wR_2 all data = 0.2699), gof = 1.016. CCDC 2184407.

2.7. [Co(NCS)$_2$(*1*)]$_n$·0.8nCHCl$_3$

$C_{52.8}H_{48.8}Cl_{2.4}CoN_{10}S_2$, M_r = 1031.55, pink block, monoclinic, space group P2$_1$/n, a = 13.3183(3), b = 12.5045(2), c = 15.2418(4) Å, β = 96.533(2)°, V = 2521.87(10) Å^3, D_c = 1.358 g cm^{-3}, T = 150 K, Z = 2, μ(CuK$_\alpha$) = 4.982 mm^{-1}. Total 22,004 reflections, 4963 unique (R_{int} = 0.0296). Refinement of 4678 reflections (377 parameters) with I > 2σ(I) converged at final R_1 = 0.1030 (R_1 all data = 0.1069), wR_2 = 0.2365 (wR_2 all data = 0.2400), gof = 0.941. CCDC 2184406.

2.8. [Co(NCS)$_2$(*2*)$_2$(MeOH)$_2$]·3CHCl$_3$

$C_{73}H_{59}Cl_9CoN_{10}O_2S_2$, M_r = 1550.40, yellow block, monoclinic, space group P2$_1$/c, a = 14.7142(9), b = 9.8420(5), c = 25.6400(17) Å, β = 94.944(5)°, V = 3699.3(4) Å^3, D_c = 1.392 g cm^{-3}, T = 150 K, Z = 2, μ(CuK$_\alpha$) = 5.755 mm^{-1}. Total 31,869 reflections, 7229 unique (R_{int} = 0.0413). Refinement of 5841 reflections (426 parameters) with I > 2σ(I) converged at final R_1 = 0.0845 (R_1 all data = 0.1041), wR_2 = 0.2057 (wR_2 all data = 0.2316), gof = 1.019. CCDC 2184410.

2.9. [Co(NCS)$_2$(*3*)]$_n$·2nCHCl$_3$

$C_{54}H_{50}Cl_6CoN_{10}S_2$, M_r = 1174.79, yellow needle, monoclinic, space group P2$_1$/n, a = 8.34220(10), b = 16.5164(3), c = 19.9774(3) Å, β = 100.0720(10)°, V = 2710.13(7) Å^3, D_c = 1.440 g cm^{-3}, T = 150 K, Z = 2, μ(CuK$_\alpha$) = 6.302 mm^{-1}. Total 27,499 reflections, 5260 unique (R_{int} = 0.0407). Refinement of 4249 reflections (334 parameters) with I > 2σ(I) converged at final R_1 = 0.0956 (R_1 all data = 0.1143), wR_2 = 0.2215 (wR_2 all data = 0.2451), gof = 1.069. CCDC 2184408.

2.10. [Co(NCS)$_2$(*4*)]$_n$

$C_{68}H_{48}CoN_{10}S_2$, M_r = 1128.21, yellow block, monoclinic, space group P2$_1$/c, a = 8.7148(3), b = 18.4121(6), c = 18.2547(5) Å, β = 101.524(2)°, V = 2870.06(16) Å^3, D_c = 1.306 g cm^{-3}, T = 150 K, Z = 2, μ(CuK$_\alpha$) = 3.430 mm^{-1}. Total 58,771 reflections, 5669 unique (R_{int} = 0.1661). Refinement of 4410 reflections (368 parameters) with I > 2σ(I) converged at final R_1 = 0.1458 (R_1 all data = 0.1614), wR_2 = 0.3652 (wR_2 all data = 0.3729), gof = 0.977. CCDC 2184409.

3. Results and Discussion

3.1. Ligand Synthesis and Characterization

Compounds **1** and **2** were prepared from 3-acetylpyridine and 4-(*N*,*N*-diethylamino) benzaldehyde or 4-(*N*,*N*-diphenylamino)benzaldehyde, respectively, using the one-pot strategy of Hanan [31]. An analogous route was used to synthesize **3** and **4**. Ligand **3** has previously been reported, but only with elemental analytical and ^{1}H NMR spectroscopic characterization [11]. Ligand **4** has also been reported and characterized [8,15]. We include additional, previously unpublished, characterization data for **3** and **4** in this report.

The MALDI mass spectra of compounds **1**–**3** are shown in Figures S1–S3 in the Supplementary Materials. The base (also the highest mass) peak corresponded to the [M + H]$^+$ ion at 381.16 for **1**, and to the M$^+$ ion at 476.13 for **2**, and at 380.18 for **3**. Solid-state IR spectra of **1**–**4** are displayed in Figures S4–S7.

The ^{1}H and ^{13}C{^{1}H} NMR spectra and the HMQC and HMBC spectra of **1**, **2**, and **3** are depicted in Figures S8–S19 in the Supplementary Materials. Additionally, COSY and NOESY spectra were recorded to aid assignment of the signals. A comparison of the aromatic regions of **1**–**3** is shown in Figure 1. The signals for H^{C2} and H^{C3} were

differentiated using NOESY H^{B3}/H^{C2} cross peaks, and NOESY H^{B3}/H^{A3} cross peaks were used to distinguish between the signals for H^{A3} and H^{A2}. The spectra are in accord with the structures shown in Scheme 2.
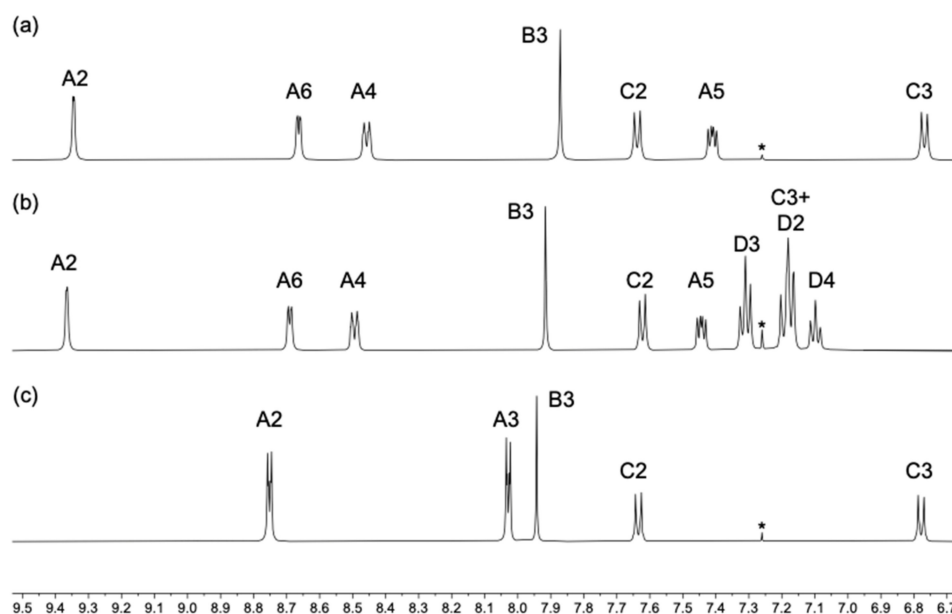

Figure 1. The aromatic regions in the ^1H NMR spectra of (**a**) **1**, (**b**) **2**, and (**c**) **3** (500 MHz, 298 K, CDCl$_3$). * = residual CHCl$_3$. Scale: δ/ppm. Atom labelling is defined in Scheme 2.

The solution absorption spectra of **1**–**3** are shown in Figure 2 and absorption maxima are given in Table 1. The more intense absorptions below 300 nm for **2** compared to **1** and **3** are consistent with the presence of the Ph$_2$N substituent in **2** versus Et$_2$N in **1** and **3**. The lower energy absorption, around 360 nm, is assigned to intra-ligand charge transfer (ILCT) involving the electron-donating Et$_2$N or Ph$_2$N substituents and electron-accepting terpyridine unit. For a CH$_2$Cl$_2$ solution of compound **4**, the corresponding absorption appears at 366 nm with ε = 25,500 dm^3 mol^{-1} cm^{-1} [15].
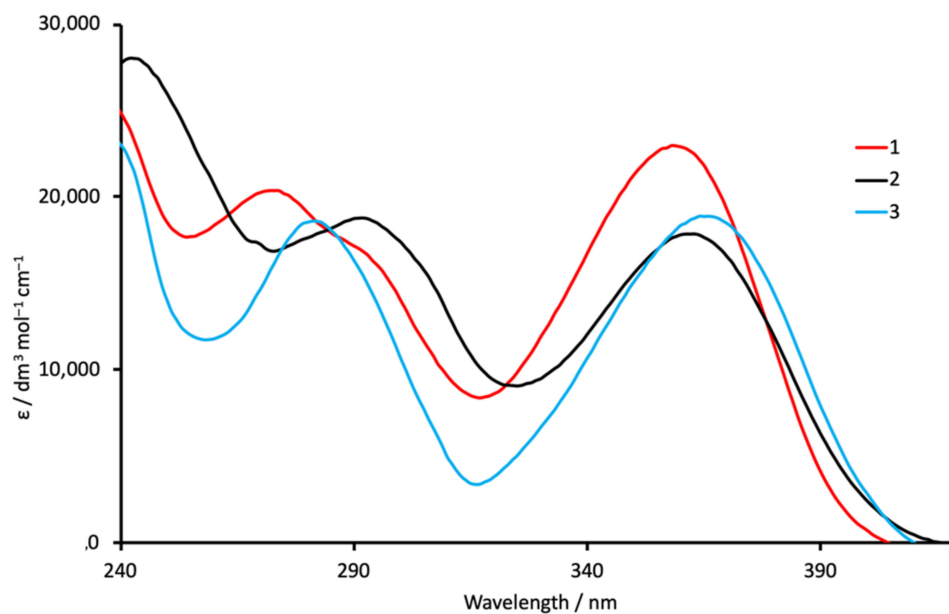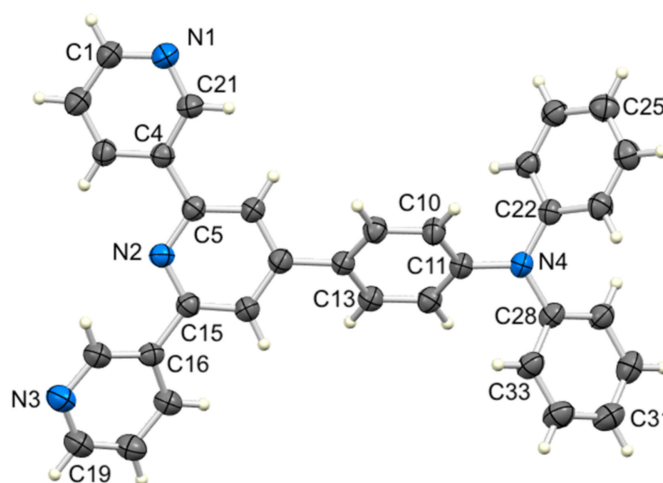

Figure 2. Solution absorption spectra of compounds **1**–**3** (CH$_2$Cl$_2$, 2×10^{-5} mol dm^{-3}).

Table 1. Solution absorption maxima of compounds **1**, **2** and **3** (CH_2Cl_2, 2×10^{-5} mol dm^{-3}).

Compound	λ_{max}/nm (ε/dm^3 mol^{-1} cm^{-1})
1	273 (20,390), 293 sh (16,600), 358 (23,000)
2	242 (28,020), 292 (18,780), 363 (17,850)
3	281 (18,590), 366 (18,870)

3.2. Single Crystal Structure of Compound 2

Yellow single crystals of **2** were obtained upon recrystallization from EtOH/CHCl$_3$ at 2–5 °C. The compound crystallizes in the monoclinic space group $C2/c$ and the molecular structure is depicted in Figure 3. Bond lengths and angles are all typical. The 3,2':6',3''-tpy unit adopts conformation **II** (Scheme 1), but deviates from planarity with the angles between the least-squares planes of the pairs of rings containing N1/N2 and N2/N3 being 11.5 and 26.1°, respectively. A larger twist angle of 39.9° is observed between the planes of the rings containing N2 and C13, consistent with alleviation of inter-ring H . . . H repulsive interactions. Atom N4 is in the expected planar environment (C22–N4–C11 = 119.1(3), C28–N4–C22 = 121.0(3), C28–N4–C11 = 119.9(3)°) and the N4–C11, N4–C22, and N4–C28 bond lengths of 1.437(5), 1.429(5), and 1.416(5) Å, respectively, are consistent with a π-contribution to each bond; the aromatic rings bonded to N4 are in a typical paddle-wheel arrangement. Packing interactions involve mainly C–H . . . π [32] contacts.

Figure 3. The structure of ligand **2** with ellipsoids plotted at a 40% probability level.

3.3. Crystal Structures of [Co(NCS)₂(1)]ₙ·0.8nCHCl₃, [Co(NCS)₂(3)]ₙ·2nCHCl₃ and [Co(NCS)₂(4)]ₙ

Single crystals of [Co(NCS)$_2$(**1**)]$_n$·0.8nCHCl$_3$, [Co(NCS)$_2$(**3**)]$_n$·2nCHCl$_3$, and [Co(NCS)$_2$(**4**)]$_n$ were grown by layering a methanol solution of Co(NCS)$_2$ over a chloroform solution of the respective ligand (see Section 2 for details). The compounds crystallize in the monoclinic spaces groups $P2_1/n$ or $P2_1/c$, and the structures of the asymmetric units in the three compounds are shown in Figure 4, as well as in Figures S20–S22 in the Supplementary Materials. Each Co atom is in an octahedral environment with the thiocyanate ligands mutually *trans* (Figure 4), and the equatorial sites occupied by N-atoms of four different terpyridine ligands (Figure 4). The variation in Co–N$_{NCS}$–C$_{NCS}$ bond angles (Table 2) is significant. A search of the Cambridge Structural Database (CSD) version 2022.1.0 [33] using Conquest version 2022.1.0 [34] for the Co^{II}–N–C–S unit reveals a range of Co–N–C angles from 93.5 to 180.0° (Figure 5). Thus, the value of 143.3(5)° observed in range shown in [Co(NCS)$_2$(**3**)]$_n$·2nCHCl$_3$ appears to be intermediate between angles associated with 'linear' and 'bent' bonding modes of the NCS$^-$ ligand. The Co–N$_{tpy}$ bond lengths are typical, and the N–Co–N bond angles (Table 2) are in accord with octahedral coordination.

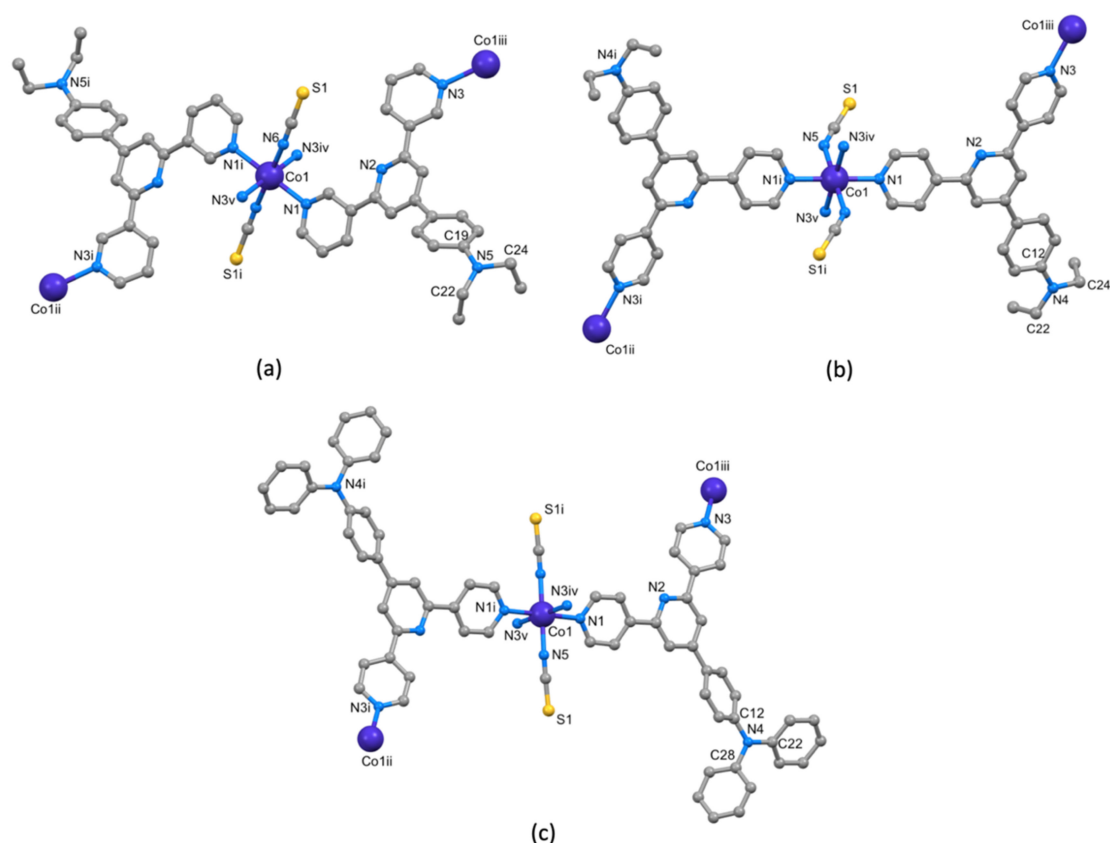**Figure 4.** Structures of the repeat units in (**a**) $[Co(NCS)_2(\mathbf{1})]_n \cdot 0.8n CHCl_3$ (symmetry codes: i = −x, 2 − y, 1 − z; ii = −$^1/_2$ − x, $^1/_2$ + y, $^1/_2$ − z; iii = $^1/_2$ − x, −$^1/_2$ + y, $^3/_2$ − z; iv = $^1/_2$ − x, $^1/_2$ + y, $^3/_2$ − z; v = −$^1/_2$ + x, $^3/_2$ − y, −$^1/_2$ + z), (**b**) $[Co(NCS)_2(\mathbf{3})]_n \cdot 2n CHCl_3$ (symmetry codes: i = 2 − x, 2 − y, 1 − z; ii = $^3/_2$ − x, $^1/_2$ + y, $^1/_2$ − z; iii = $^5/_2$ − x, −$^1/_2$ + y, $^3/_2$−z; iv = $^5/_2$−x, $^1/_2$ + y, $^3/_2$ − z; v = −$^1/_2$ +x, $^3/_2$ − y, −$^1/_2$ + z), and (**c**) $[Co(NCS)_2(\mathbf{4})]_n$ (symmetry codes: i = 1 − x, 1−y, 1 − z; ii = 1 − x, −$^1/_2$ + y, $^1/_2$−z; iii = 1−x, $^1/_2$+ y, $^3/_2$−z; iv = x, $^3/_2$ − y, −$^1/_2$ + z; v = 1 − x, −$^1/_2$ − y, $^3/_2$ + z).

Table 2. Selected bond lengths and angles in $[Co(NCS)_2(\mathbf{1})]_n \cdot 0.8n CHCl_3$, $[Co(NCS)_2(\mathbf{3})]_n \cdot 2n CHCl_3$ and $[Co(NCS)_2(\mathbf{4})]_n$.

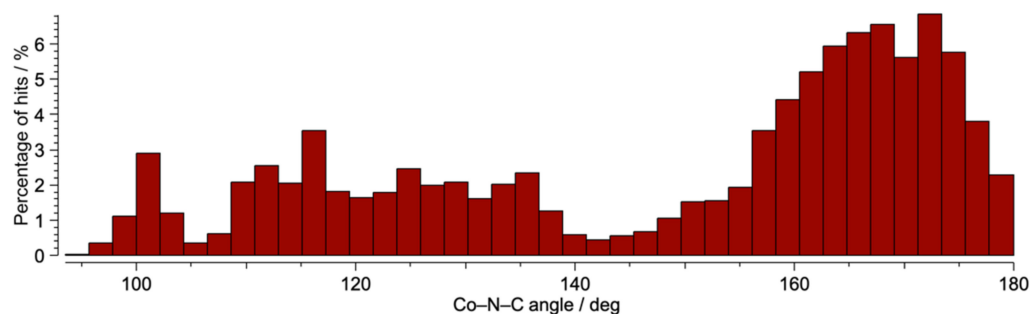| Compound	Co–N_{NCS}/Å	Co–N_{tpy}/Å	Co–N_{NCS}–C_{NCS}/°	Range of N–Co–N [a]/°
$[Co(NCS)_2(\mathbf{1})]_n \cdot 0.8n CHCl_3$	2.078(4)	2.211(4), 2.205(4)	164.9(4)	89.07(15)–90.93(15)
$[Co(NCS)_2(\mathbf{3})]_n \cdot 2n CHCl_3$	2.085(4)	2.194(4), 2.230(4)	143.3(5)	86.32(15)–93.68(15)
$[Co(NCS)_2(\mathbf{4})]_n$	2.076(8)	2.186(7), 2.202(7)	163.7(7)	86.4(3)–93.6(3)

[a] Only *cis* angles are given.

Figure 5. Distribution of Co–N_{NCS}–C_{NCS} bond angles in compounds containing *N*-bonded thiocyanate ligands coordinated to cobalt(II) found in the CSD (version 2022.1.0).

In [Co(NCS)$_2$(**1**)]$_n$·0.8nCHCl$_3$, the 3,2':6',3''-tpy unit exhibits conformation **II** (Figure 4a and Scheme 1), while in [Co(NCS)$_2$(**3**)]$_n$·2nCHCl$_3$ and [Co(NCS)$_2$(**4**)]$_n$, only one limiting planar conformation of the 4,2':6',4''-tpy domain is possible. In each case, the structure propagates into a (4,4) net, directed by 4-connecting Co(II) nodes. Part of each net is shown in Figure 6, with the Co....Co vectors highlighted in blue. Each rhombus in each network is defined by four Co atoms and four ligands, with the 4-(N,N-diethylamino)phenyl or 4-(N,N-diphenylamino)phenyl substituents directed above or below the plane defined by the Co atoms. Working around each rhombus, an 'up–up–down–down' arrangement of substituents is observed. Internal angles in each rhombus in [Co(NCS)$_2$(**1**)]$_n$·0.8nCHCl$_3$ are 66.5 and 113.5°, while the corresponding angles in [Co(NCS)$_2$(**3**)]$_n$·2nCHCl$_3$ and [Co(NCS)$_2$(**4**)]$_n$ are 78.4 and 101.6°, and 89.5 and 90.5°, respectively. A comparison of Figure 6a,b reveals how the change from a 3,2':6',3''- to 4,2':6',4''-tpy unit affects the orientation of the 4-(diethylamino)phenyl substituents. The effects of going from 4-(N,N-diethylamino)phenyl to 4-(N,N-diphenylamino)phenyl substituents, while maintaining a common 4,2':6',4''-tpy metal-binding domain, can be appreciated by comparing Figure 6b with 6c.
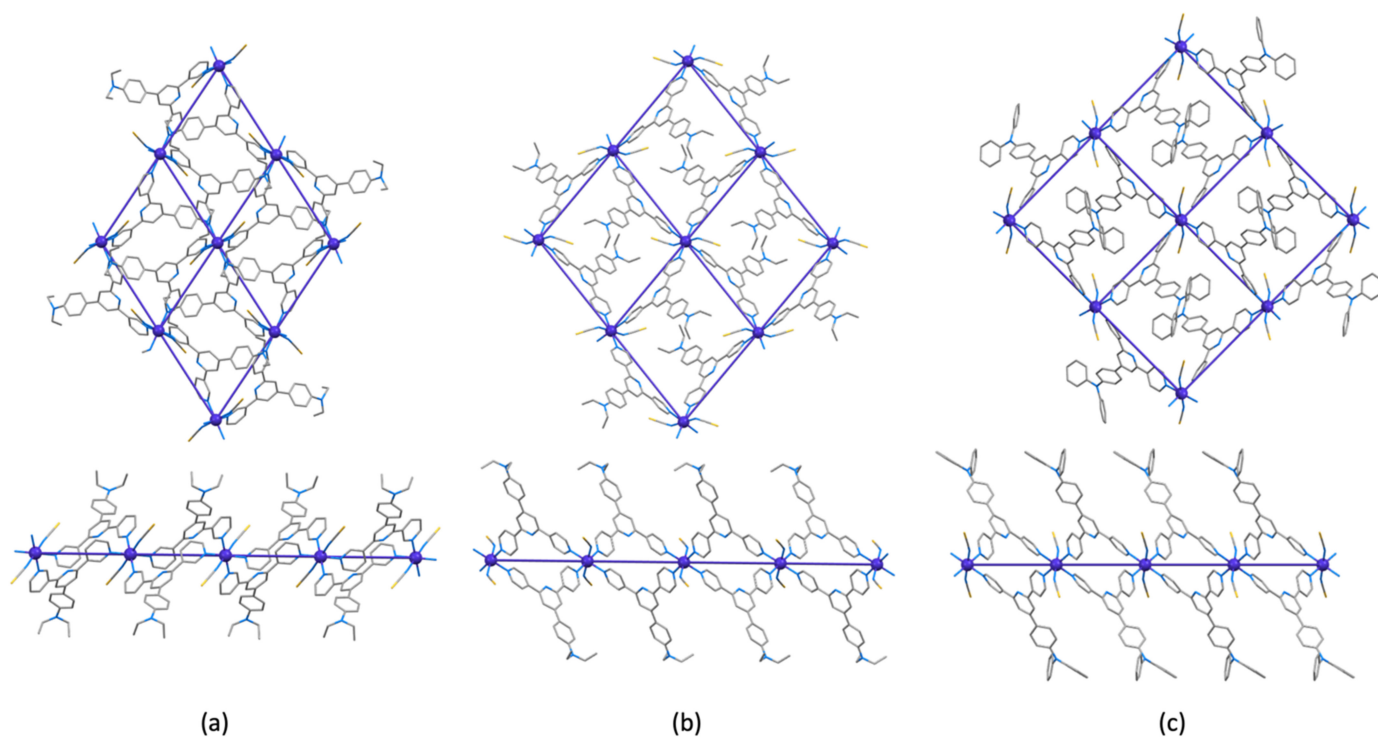

(a) (b) (c)

Figure 6. The (4,4) net (**top**) and a view down the *b*-axis (**bottom**) in (**a**) [Co(NCS)$_2$(**1**)]$_n$·0.8nCHCl$_3$, (**b**) [Co(NCS)$_2$(**3**)]$_n$·2nCHCl$_3$, and (**c**) [Co(NCS)$_2$(**4**)]$_n$. The Co....Co vectors are depicted as blue lines to aid visualization of the (4,4) nets.

In each compound, the Co atoms in the (4,4) net lie in a plane. In [Co(NCS)$_2$(**1**)]$_n$·0.8nCHCl$_3$, the inter-plane distances are 10.58 Å, and the 4-(N,N-diethylamino)phenyl groups are accommodated between the sheets, leaving cavities within the Co-containing planes which are occupied by CHCl$_3$ molecules. A change from ligand **1** to **3** (i.e., 3,2':6',3''-tpy to 4,2':6',4''-tpy units), while retaining the same 4'-substituent, results in a closer approach of the Co-containing layers (inter-plane distance = 8.10 Å). As a result, the Et$_2$N groups penetrate into cavities in an adjacent sheet. Despite this, the solvent-accessible void space increases from ca. 9.4% in [Co(NCS)$_2$(**1**)]$_n$ to 18.2% in [Co(NCS)$_2$(**3**)]$_n$; these were calculated using Mercury 2022.1.0 [26] with a probe radius of 1.2 Å, and this is consistent with the reported formulae of [Co(NCS)$_2$(**1**)]$_n$·0.8nCHCl$_3$ and [Co(NCS)$_2$(**3**)]$_n$·2nCHCl$_3$. In [Co(NCS)$_2$(**4**)]$_n$, the inter-plane separation is 8.54 Å. The 4-(N,N-diphenylamino)phenyl substituents in one sheet penetrate through the adjacent sheet (Figure 7a) and engage in an

embrace [35,36] with another 4-(*N*,*N*-diphenylamino)phenyl from the next-but-one sheet (Figure 7b). The packing is efficient, leaving no solvent-accessible voids.
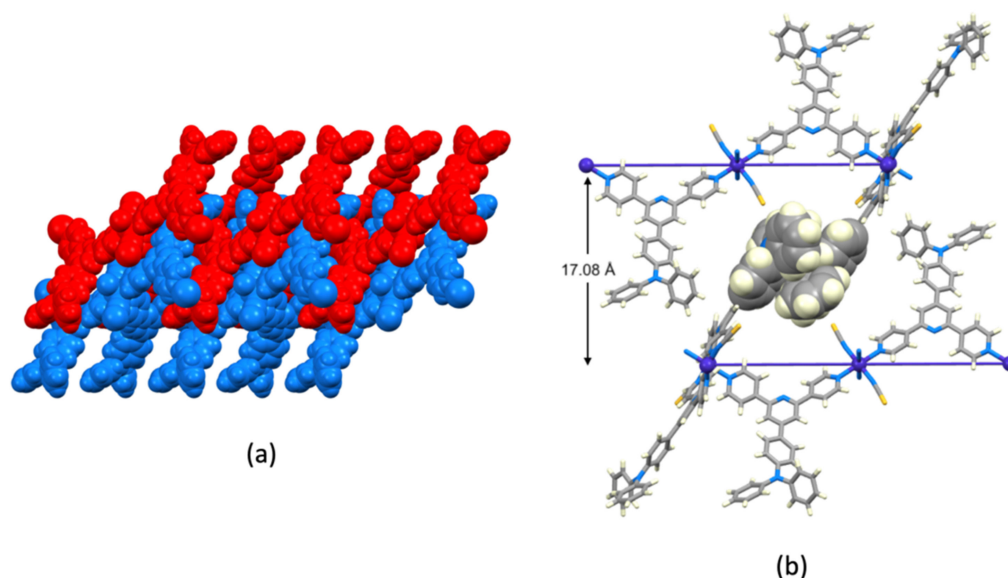

Figure 7. (**a**) Packing of adjacent sheets in the crystal lattice of [Co(NCS)$_2$(**4**)]$_n$ (viewed down the *b*-axis). (**b**) Pairs of 4-(*N*,*N*-diphenylamino)phenyl groups (space-filling representation) in non-adjacent sheets engage in an embrace; 17.08 Å = twice the inter-plane separation of adjacent sheets.

The bulk samples from the crystallization tubes, from which single crystals of [Co(NCS)$_2$(**1**)]$_n$·0.8*n*CHCl$_3$, [Co(NCS)$_2$(**3**)]$_n$·2*n*CHCl$_3$, and [Co(NCS)$_2$(**4**)]$_n$ were harvested, were analysed by IR spectroscopy and PXRD. The IR spectra are displayed in Figures S23–S25 (see the Supplementary Materials) and exhibit strong absorptions at 2070, 2049, and 2060 cm^{-1} for [Co(NCS)$_2$(**1**)]$_n$·0.8*n*CHCl$_3$, [Co(NCS)$_2$(**3**)]$_n$·2*n*CHCl$_3$, and [Co(NCS)$_2$(**4**)]$_n$, respectively, which are assigned to the CN stretching modes of the coordinated thiocyanate ligands. The region around 3000 cm^{-1}, and the fingerprint region of each spectrum, is characteristic of ligand **1**, **3**, or **4** (compare with Figures S4, S6, and S7). Experimental PXRD patterns were compared with those predicted from the single crystal data, and provided good matches for all three compounds, confirming that the single crystal structures were representative of the bulk materials. PXRD patterns up to 2θ = 50° are given in Figure 8, and full PXRD patterns are shown in Figures S26–S28 in Supplementary Materials.

3.4. Crystal Structure of [Co(NCS)$_2$(**2**)$_2$(MeOH)$_2$]·3CHCl$_3$

Unexpectedly, the reaction of ligand **2** with Co(NCS)$_2$ led to the discrete molecular complex [Co(NCS)$_2$(**2**)$_2$(MeOH)$_2$]·3CHCl$_3$. The compound crystallizes in the monoclinic $P2_1/c$ space group, and Figure 9 and Figure S29 depict the structure. Atom Co1 is located on an inversion centre, and the asymmetric unit contains one crystallographic independent ligand **2**. The Co–N$_{tpy}$, Co–N$_{NCS}$, and Co–O bond lengths of 2.190(3), 2.090(4), and 2.083(3) Å, respectively, are typical, and N–Co–N and N–Co–O bond angles lie in the range of 87.84(13) to 92.16(13)°. The NCS$^-$ ligand coordinates in a linear mode (Co1–N5–C36 = 176.2(4)°). The 3,2″:6′,3″-tpy unit adopts conformation **I** (Scheme 1), with angles between the least-squares planes of the pyridine rings containing N1/N2 and N2/N3 being 32.4 and 5.1°. The arene ring containing C15 is twisted through 24.9° with respect to the pyridine ring with N2. This is smaller than the 39.9° angle observed in the free ligand **2**.
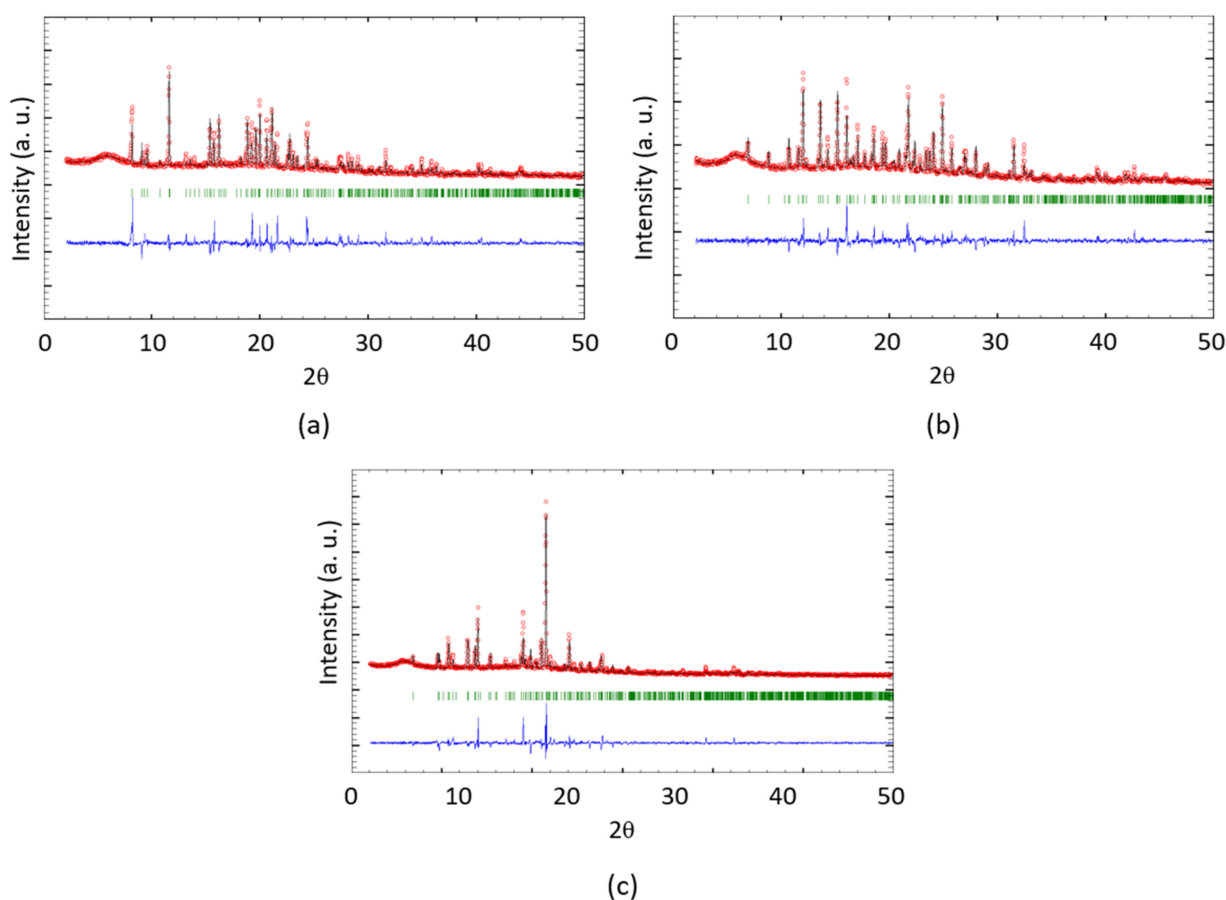
Figure 8. PXRD (CuKα1 radiation) patterns for (**a**) [Co(NCS)$_2$(**1**)]$_n$·0.8*n*CHCl$_3$, (**b**) [Co(NCS)$_2$(**3**)]$_n$·2*n*CHCl$_3$, and (**c**) [Co(NCS)$_2$(**4**)]$_n$ up to 2θ = 50°. The experimental pattern (red circles) is compared with the best fit from the Rietveld refinement analysis (black line). Bragg peak positions (green) and differences between the calculated and experimental plots (blue) are shown.
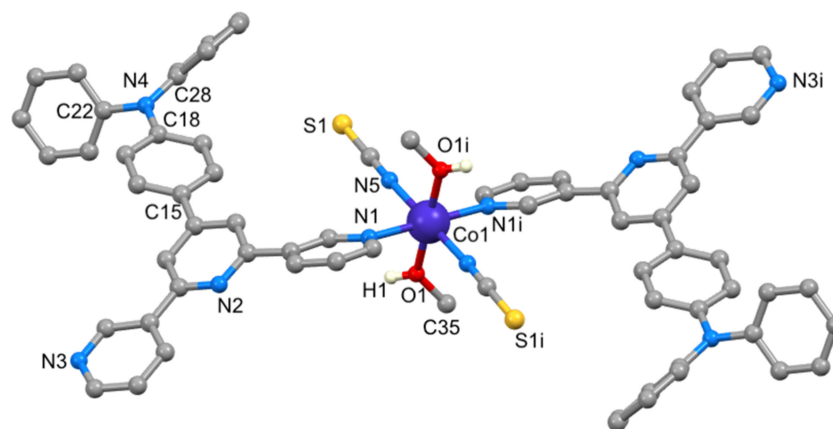

Figure 9. Structure of the [Co(NCS)$_2$(**2**)$_2$(MeOH)$_2$] complex in the CHCl$_3$ solvate; H atoms are omitted (symmetry code i = 2 − *x*, −*y*, 1 − *z*).

While N1 is coordinated to Co1, the non-coordinated atom N3 is involved in a hydrogen-bonded interaction to the coordinated MeOH molecule of an adjacent [Co(NCS)$_2$(**2**)$_2$(MeOH)$_2$] complex. This leads to the assembly of 1D-chains supported by hydrogen bonds (Figure 10a). Relevant bond parameters are N3....H1^{ii} = 1.84(3) Å, N3....O1^{ii} = 2.688(4) Å, angle N3....H1^{ii}–O1^{ii} = 180(3)°. The chains are further supported by face-to-face π-stacking interactions between pyridine rings containing N2 and N3^{ii}, and the pair

symmetry-related pair with N3 and N2^{ii} (Figure 10b, angle between ring planes = 5.1° and centroid...centroid = 4.03 Å).
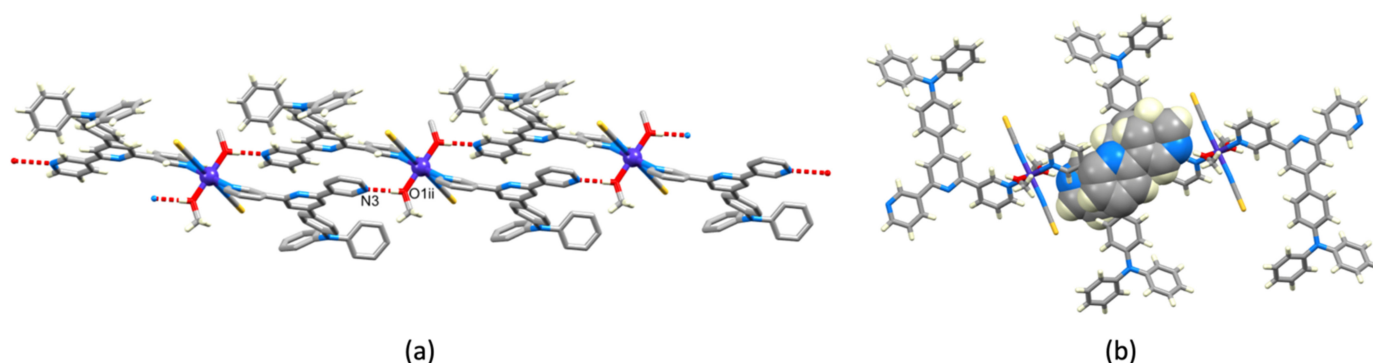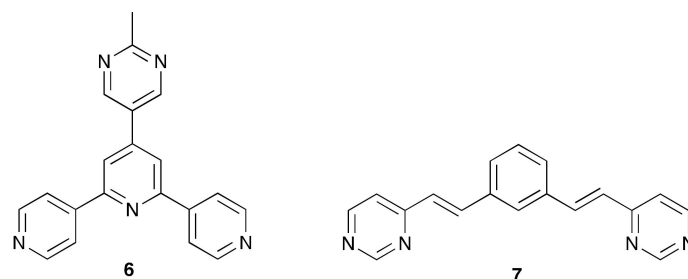

(a)　　　　　　　　　　　　　　　　　　　　　　　　(b)

Figure 10. (**a**) Part of one hydrogen-bonded 1D-chain in [Co(NCS)$_2$(**2**)$_2$(MeOH)$_2$]·3CHCl$_3$ (symmetry code ii = $1 - x$, $-y$, $1 - z$), and (**b**) the π-stacking interaction between pairs of terpyridine units within the chain.

The solid-state IR spectrum (Figure S30 in Supplementary Materials) of the bulk sample from the crystallization tube from the reaction of **2** and Co(NCS)$_2$ exhibits a characteristic, strong absorption at 2078 cm^{-1}, arising from the CN stretch of the coordinated NCS$^-$ ligands. The bulk material was also analysed by PXRD, and the match between the experimental powder pattern and that predicted from the single-crystal structure determination (Figure 11) confirmed that the single-crystal structure was representative of the bulk sample. The non-innocent role of MeOH in the formation of [Co(NCS)$_2$(**2**)$_2$(MeOH)$_2$] is reminiscent of the assembly of [Co(NCS)$_2$(**5**)(MeOH)$_2$]$_n$, in which **5** is 4′-(4-methoxyphenyl)-3,2′:6′,3′′-terpyridine [21]. The Co(II) centre in [Co(NCS)$_2$(**5**)(MeOH)$_2$]$_n$ is in the same *trans*-{Co(NCS)$_2$(MeOH)$_2$(N$_{tpy}$)$_2$} environment as in [Co(NCS)$_2$(**2**)$_2$(MeOH)$_2$]. However, ligand **5** coordinates through both outer pyridine rings to produce a 1D-coordination polymer. Similarly, the reaction of Co(NCS)$_2$ with 2,5-dimethylpyrazine (Me$_2$pyz) in MeOH resulted in the assembly of the 1D-polymer [Co(NCS)$_2$(Me$_2$pyz)(MeOH)$_2$]$_n$ [37], and layering of a MeOH solution of Co(NCS)$_2$ over a CHCl$_3$ solution of **6** (Scheme 3) led to the 1D-polymer [Co(NCS)$_2$(**6**)(MeOH)$_2$]$_n$ [38]. The factors that control the assembly of a polymer versus a discrete molecular complex with pendant N-donors are unclear. For example, layering of a MeOH solution of **7** (Scheme 3) over an aqueous solution of Co(NCS)$_2$ resulted in the formation of the molecular complex [Co(NCS)$_2$(**7**)$_2$(MeOH)$_2$], which is closely related to [Co(NCS)$_2$(**2**)$_2$(MeOH)$_2$]; [Co(NCS)$_2$(**7**)$_2$(MeOH)$_2$] also forms hydrogen-bonded chains in the solid state [39]. These examples are representative of a significant number of structurally characterized [33,34] coordination compounds, both molecular and polymeric, which contain a *trans*-{Co(NCS)$_2$(MeOH)$_2$(N)$_2$} motif.

Scheme 3. Structures of ligands **6** and **7** [38,39].

Figure 11. PXRD (CuKα1 radiation) patterns for $[Co(NCS)_2(\mathbf{2})_2(MeOH)_2]\cdot3CHCl_3$ up to $2\theta = 50°$. The experimental pattern (red circles) is matched with the best fit from the Rietveld refinement analysis (black line). Bragg peak positions (green) and differences between the calculated and experimental plots (blue) are also shown. See Figure S30 for the complete PXRD.

4. Conclusions

We have prepared and characterized compounds **1** and **2**, which contain $3,2':6',3''$-tpy metal-binding domains and peripheral 4-(*N,N*-diethylamino)phenyl or 4-(*N,N*-dipheny lamino)phenyl groups. Ligands **1** and **2**, along with their $4,2':6',4''$-tpy analogues, **3** and **4**, were reacted with $Co(NCS)_2$ by layering MeOH solutions of the cobalt(II) salt over $CHCl_3$ solutions of the ligands. The single-crystal structures of $[Co(NCS)_2(\mathbf{1})]_n\cdot0.8nCHCl_3$, $[Co(NCS)_2(\mathbf{3})]_n\cdot2nCHCl_3$, and $[Co(NCS)_2(\mathbf{4})]_n$ confirmed the assembly of 2D (4,4) nets, with each Co(II) centre acting as a 4-connecting node. Ligand **1** adopts conformation **II** (Scheme 1) in $[Co(NCS)_2(\mathbf{1})]_n\cdot0.8nCHCl_3$. Going from $[Co(NCS)_2(\mathbf{1})]_n\cdot0.8nCHCl_3$ ($3,2':6',3''$-tpy) to $[Co(NCS)_2(\mathbf{3})]_n\cdot2nCHCl_3$ ($4,2':6',4''$-tpy) leads to a closer approach of the Co-containing sheets; the inter-plane distance decreases from 10.58 Å to 8.10 Å, and this is accompanied by an increase in the solvent-accessible void space from 9.4% in $[Co(NCS)_2(\mathbf{1})]_n$ to 18.2% in $[Co(NCS)_2(\mathbf{3})]_n$. The 2D-sheets in $[Co(NCS)_2(\mathbf{4})]_n$ feature embracing pairs of 4-(diphenylamino)phenyl substituents, which occur between non-adjacent nets. The reaction between **2** and $Co(NCS)_2$ in $CHCl_3/MeOH$ leads to the molecular complex $[Co(NCS)_2(\mathbf{2})_2(MeOH)_2]$, which assembles into a 1D-polymer through hydrogen bonding, illustrating the non-innocent role of MeOH as a solvent. PXRD of bulk samples of all four products confirmed the single-crystal structures as representative of the bulk materials.

References

1. Housecroft, C.E. 4,2′:6′,4″-Terpyridines: Diverging and diverse building blocks in coordination polymers and metallomacrocycles. *Dalton Trans.* **2014**, *43*, 6594–6604. [CrossRef] [PubMed]
2. Housecroft, C.E. Divergent 4,2′:6′,4″- and 3,2′:6′,3″-terpyridines as linkers in 2- and 3-dimensional architectures. *CrystEngComm* **2015**, *17*, 7461–7468. [CrossRef]
3. Housecroft, C.E.; Constable, E.C. The terpyridine isomer game: From chelate to coordination network building block. *Chem. Commun.* **2020**, *56*, 10786–10794. [CrossRef]
4. Housecroft, C.; Constable, E. Isomers of Terpyridine as Ligands in Coordination Polymers and Networks Containing Zinc(II) and Cadmium(II). *Molecules* **2021**, *26*, 3110. [CrossRef] [PubMed]
5. Zhang, J.; Wang, H. Photophysical investigaions and the bioimaings of α-, β-, γ-pyridine-based terpyridine derivatives. *J. Mol. Struct.* **2018**, *1157*, 457–462. [CrossRef]
6. Zhang, J.; Abudoureheman, M.; Lian, Z.; Liu, J.; Wu, Q.; Xuan, X. Controllable Synthesis of Centrosymmetric/Noncentrosymmetric Phases for the Family of Halogen-Based Photonic Coordination Polymers to Enhance the Phase-Matching Second-Harmonic-Generation Response. *Inorg. Chem.* **2022**, *61*, 3716–3722. [CrossRef] [PubMed]
7. Jia, R.; Zhu, Y.; Hu, L.; Xiong, Q.; Zhao, M.; Zhang, M.; Tian, X. A series of terpyridine containing flexible amino diethylacetate derivatives with large two-photon action cross-sections for effective mitochondrial imaging in living liver cancerous cells. *Spectrochim. Acta Part A* **2018**, *188*, 633–639. [CrossRef]
8. Li, L.; Liu, E.; Cheng, J.; Zhang, G. Iron(ii) coordination polymer catalysed hydroboration of ketones. *Dalton Trans.* **2018**, *47*, 9579–9584. [CrossRef] [PubMed]
9. Zhang, G.; Jia, Y.-X.; Chen, W.; Lo, W.-F.; Brathwaite, N.; Golen, J.A.; Rheingold, A.L. Diverse zinc(ii) coordination assemblies built on divergent 4,2′:6′,4″-terpyridine derivatives: Syntheses, structures and catalytic properties. *RSC Adv.* **2015**, *5*, 15870–15879. [CrossRef]
10. Zhang, G.; Tan, J.; Phoenix, T.; Manke, D.R.; Golen, J.A.; Rheingold, A.L. Amalgamating 4′-substituted 4,2′:6′,4″-terpyridine ligands with double-helical chains or ladder-like networks. *RSC Adv.* **2016**, *6*, 9270–9277. [CrossRef]
11. Sotnik, S.A.; Polunin, R.A.; Kiskin, M.A.; Kirillov, A.M.; Dorofeeva, V.N.; Gavrilenko, K.S.; Eremenko, I.L.; Novotortsev, V.M.; Kolotilov, S.V. Heterometallic Coordination Polymers Assembled from Trigonal Trinuclear Fe₂Ni-Pivalate Blocks and Polypyridine Spacers: Topological Diversity, Sorption, and Catalytic Properties. *Inorg. Chem.* **2015**, *54*, 5169–5181. [CrossRef] [PubMed]
12. Yuan, F.; Wang, X.; Hu, H.-M.; Shen, S.-S.; An, R.; Xue, G. Syntheses, structures and luminescent properties of two new zinc coordination polymers based on 4′-(4-aminephenyl)-4,2′:6′,4″-terpyridine. *Inorg. Chem. Commun.* **2014**, *48*, 26–29. [CrossRef]
13. Li, L.; Zhang, Y.Z.; Yang, C.; Liu, E.; Golen, J.A.; Zhang, G. One-dimensional copper(II) coordination polymers built on 4′-substituted 4,2′:6′,4″- and 3,2′:6′,3″-terpyridines: Syntheses, structures and catalytic properties. *Polyhedron* **2016**, *105*, 115–122. [CrossRef]
14. Constable, E.C.; Zhang, G.; Housecroft, C.E.; Neuburger, M.; Zampese, J.A. Sheet, ladder or chain? Small substituents in 4′-phenyl-4,2′:6′,4″-terpyridines control dimensionality in cadmium(ii) coordination polymers. *CrystEngComm* **2010**, *12*, 3733–3739. [CrossRef]
15. Su, J.; Zhang, J.; Tian, X.; Zhao, M.; Song, T.; Yu, J.; Cui, Y.; Qian, G.; Zhong, H.; Luo, L.; et al. A series of multifunctional coordination polymers based on terpyridine and zinc halide: Second-harmonic generation and two-photon absorption properties and intracellular imaging. *J. Mater. Chem. B* **2017**, *5*, 5458–5463. [CrossRef]
16. Constable, E.C.; Housecroft, C.E.; Neuburger, M.; Vujovic, S.; Zampese, J.A.; Zhang, G. Cobalt(ii) coordination polymers with 4′-substituted 4,2′:6′,4″- and 3,2′:6′,3″-terpyridines: Engineering a switch from planar to undulating chains and sheets. *CrystEngComm* **2012**, *14*, 3554–3563. [CrossRef]
17. Rocco, D.; Prescimone, A.; Constable, E.C.; Housecroft, C.E. Directing 2D-Coordination Networks: Combined Effects of a Conformationally Flexible 3,2′:6′,3″-Terpyridine and Chain Length Variation in 4′-(4-n-Alkyloxyphenyl) Substituents. *Molecules* **2020**, *25*, 1663. [CrossRef]
18. Rocco, D.; Prescimone, A.; Constable, E.C.; Housecroft, C.E. Adapting (4,4) Networks through Substituent Effects and Conformationally Flexible 3,2′:6′,3″-Terpyridines. *Molecules* **2021**, *26*, 6337. [CrossRef]
19. Rocco, D.; Prescimone, A.; Constable, E.C.; Housecroft, C.E. Straight Versus Branched Chain Substituents in 4′-(Butoxyphenyl)-3,2′:6′,3″-terpyridines: Effects on (4,4) Coordination Network Assemblies. *Polymers* **2020**, *12*, 1823. [CrossRef]
20. Rocco, D.; Novak, S.; Prescimone, A.; Constable, E.C.; Housecroft, C.E. Coordination networks assembled from Co(NCS)2 and 4′-[4-(naphthalen-1-yl)phenyl]-3,2′:6′,3″-terpyridine: Role of lattice solvents. *Polyhedron* **2021**, *208*, 115445. [CrossRef]
21. Rocco, D.; Prescimone, A.; Klein, Y.M.; Gawryluk, D.J.; Constable, E.C.; Housecroft, C.E. Competition in Coordination Assemblies: 1D-Coordination Polymer or 2D-Nets Based on Co(NCS)2 and 4′-(4-methoxyphenyl)-3,2′:6′,3″-terpyridine. *Polymers* **2019**, *11*, 1224. [CrossRef] [PubMed]
22. Palatinus, L.; Chapuis, G. SUPERFLIP— A computer program for the solution of crystal structures by charge flipping in arbitrary dimensions. *J. Appl. Crystallogr.* **2007**, *40*, 786–790. [CrossRef]
23. Palatinus, L.; Prathapa, S.J.; van Smaalen, S. *EDMA*: A computer program for topological analysis of discrete electron densities. *J. Appl. Crystallogr.* **2012**, *45*, 575–580. [CrossRef]
24. Dolomanov, O.V.; Bourhis, L.J.; Gildea, R.J.; Howard, J.A.K.; Puschmann, H. OLEX2: A complete structure solution, refinement and analysis program. *J. Appl. Crystallogr.* **2010**, *42*, 339–341. [CrossRef]

25. Sheldrick, G.M. Crystal structure refinement with *SHELXL*. *Acta Crystallogr. Sect. C Struct. Chem.* **2015**, *C27*, 3–8. [CrossRef] [PubMed]

26. Macrae, C.F.; Sovago, I.; Cottrell, S.J.; Galek, P.T.A.; McCabe, P.; Pidcock, E.; Platings, M.; Shields, G.P.; Stevens, J.S.; Towler, M.; et al. Mercury 4.0: From visualization to analysis, design and prediction. *J. Appl. Crystallogr.* **2020**, *53*, 226–235. [CrossRef] [PubMed]

27. Le Bail, A.; Duroy, H.; Fourquet, J. Ab-initio structure determination of LiSbWO6 by X-ray powder diffraction. *Mater. Res. Bull.* **1988**, *23*, 447–452. [CrossRef]

28. Pawley, G.S. Unit-cell refinement from powder diffraction scans. *J. Appl. Crystallogr.* **1981**, *14*, 357–361. [CrossRef]

29. Rodríguez-Carvajal, J. Recent advances in magnetic structure determination by neutron powder diffraction. *Phys. B Condens. Matter* **1993**, *192*, 55–69. [CrossRef]

30. Roisnel, T.; Rodríguez-Carvajal, J. WinPLOTR: A Windows tool for powder diffraction patterns analysis Materials Science Forum. In Proceedings of the Seventh European Powder Diffraction Conference (EPDIC 7), Barcelona, Spain, 20–23 May 2000; pp. 118–123.

31. Hanan, G.S.; Wang, J. A Facile Route to Sterically Hindered and Non-Hindered 4′-Aryl-2,2′:6′,2′′-Terpyridines. *Synlett* **2005**, 251–1254. [CrossRef]

32. Nishio, M. CH/π hydrogen bonds in crystals. *CrystEngComm* **2004**, *6*, 130–158. [CrossRef]

33. Groom, C.R.; Bruno, I.J.; Lightfoot, M.P.; Ward, S.C. The Cambridge Structural Database. *Acta Crystallogr. Sect. B Struct. Sci. Cryst. Eng. Mater.* **2016**, *B72*, 171–179. [CrossRef]

34. Bruno, I.J.; Cole, J.C.; Edgington, P.R.; Kessler, M.; Macrae, C.F.; McCabe, P.; Pearson, J.; Taylor, R. New software for searching the Cambridge Structural Database and visualizing crystal structures. *Acta Crystallogr. Sect. B Struct. Sci.* **2002**, *58*, 389–397. [CrossRef] [PubMed]

35. Dance, I.; Scudder, M. Supramolecular Motifs: Concerted Multiple Phenyl Embraces between Ph_4P^+ Cations Are Attractive and Ubiquitous. *Chem. Eur. J.* **1996**, *2*, 481–486. [CrossRef] [PubMed]

36. Dance, I.; Scudder, M. The sextuple phenyl embrace, a ubiquitous concerted supramolecular motif. *J. Chem. Soc. Chem. Commun.* **1995**, 1039–1040. [CrossRef]

37. Suckert, S.; Jess, I.; Näther, C. Synthesis, Structures, and Thermal Properties of Cobalt(II) Thiocyanate Coordination Compounds with 2,5-Dimethylpyrazine. *Z. Anorg. Allg. Chem.* **2017**, *643*, 721–728. [CrossRef]

38. Klein, Y.M.; Prescimone, A.; Constable, E.C.; Housecroft, C.E. 4,2′:6′,4′′- and 3,2′:6′,3′′-Terpyridines: The Conflict between Well-Defined Vectorial Properties and Serendipity in the Assembly of 1D-, 2D- and 3D-Architectures. *Materials* **2017**, *10*, 728. [CrossRef] [PubMed]

39. Shin, D.M.; Lee, A.I.S.; Chung, Y.K. Self-Assemblies of New Rigid Angular Ligands and Metal Centers toward the Rational Construction and Modification of Novel Coordination Polymer Networks. *Inorg. Chem.* **2003**, *42*, 8838–8846. [CrossRef] [PubMed]